ACS Sustainable Chemistry & Engineering

Research Article

pubs.acs.org/journal/ascecg

Carbon-Nanotube-Incorporated Graphene Scroll-Sheet Conjoined Aerogels for Efficient Hydrogen Evolution Reaction

Yiqin Shi,[†] Wei Gao,[‡] Hengyi Lu,[‡] Yunpeng Huang,[‡] Lizeng Zuo,[‡] Wei Fan,*[,†] and Tianxi Liu*[,†,‡]

[†]State Key Laboratory for Modification of Chemical Fibers and Polymer Materials, College of Materials Science and Engineering, Donghua University, 2999 North Renmin Road, Shanghai 201620, P. R. China

[‡]State Key Laboratory of Molecular Engineering of Polymers, Department of Macromolecular Science, Fudan University, 220 Handan Road, Shanghai 200433, P. R. China

Supporting Information

ABSTRACT: Developing low-cost Pt-free hydrogen evolution reaction (HER) electrocatalyst is highly desired in exploiting hydrogen as a sustainable new energy carrier. Herein, hierarchically structured graphene-carbon nanotube aerogel-$MoSe_2$ hybrid (GCA-$MoSe_2$) was constructed as efficient HER electrocatalysts. GCA was facilely fabricated by direct freeze-drying of graphene oxide (GO)-carbon nanotube (CNT) hybrid dispersion, with subsequent carbonization. Through a shock cooling method, a unique scroll-sheet conjoined architecture could be formed in GCA, which can function as highly conductive skeleton, thus facilitating the transport of electrons through the whole hybrids. Furthermore, CNTs acting as "spacers" between graphene layers can efficiently impede their restacking, thus giving full play to the superior electrical conductivity of graphene. The hierarchical porous aerogel skeleton could allow full impregnation of electrolyte, accelerating the ion diffusion kinetics. Benefiting from the three-dimensional (3D) network of GCA, $MoSe_2$ nanosheets can grow densely and perpendicularly on the aerogel, preventing them from aggregation to maximize the number of catalytic active sites on the edges. The ensemble of these benefits makes the hybrid an efficient electrocatalyst for HER, which exhibits an onset potential of 113 mV, small Tafel slope of 68 mV decade^{-1} and good stability. Such a simple method of immobilizing guest nanosheets/particles in the host of GCA opens a new avenue for manufacturing macroscopic electrode materials in large scale.

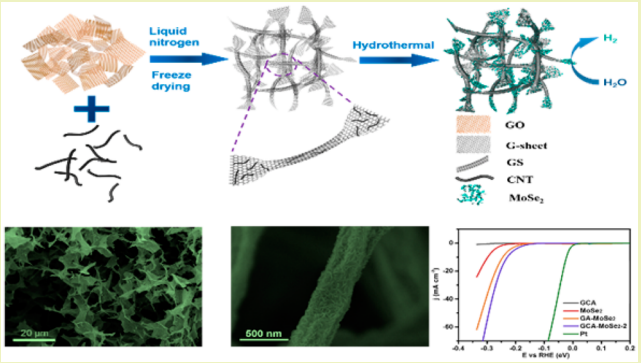

KEYWORDS: *$MoSe_2$, Graphene−carbon nanotube aerogel, Scroll-sheet conjoined, Hydrogen evolution reaction*

INTRODUCTION

Hydrogen, as one of the most promising sustainable energy carrier to substitute fossil fuels, has drawn tremendous attentions. Splitting water by using electricity is a green way to produce hydrogen.[1] Although platinum (Pt)-based material is most effective in electrocatalyzing hydrogen evolution reaction (HER), the high cost and scarcity of Pt has driven the research on exploring earth-abundant and high performance catalysts.[2] The layered transitional-metal dichalcogenide (TMD) MX_2, where M represents transitional metal and X represents S, Se, or Te, has been extensively investigated as alternatives to Pt type catalysts because of the low cost and high electrocatalytic activity.[3−5] The ultrathin architecture of TMD is favorable for exposing those active sites located on edges to catalyze HER.[6,7] $MoSe_2$, as one of the newly emerging TMD, exhibits high catalytic activity derived from the selenium edge sites, as well as good durability in acidic environment.[8,9] However, the inevitable agglomeration and stacking of nanosheets in bulk material could inevitably hinder the number of catalytic sites, while the intrinsic low conductivity of pure $MoSe_2$ impedes the ion/electron transport and limits the catalytic activity. Coupling $MoSe_2$ nanosheets with carbon support has been proposed as an effective solution to stabilize the layered structure of $MoSe_2$ during the synthesis and improve the electrical contact to the electrode. Several reports have proved that the integration of $MoSe_2$ with carbon substrates like carbon nanotubes,[10] graphene,[11,12] carbon fiber cloth[13] or cotton-derived carbon fiber aerogel[14] could promote its catalytic performance.

Three-dimensional (3D) carbon framework like graphene aerogel, possessing large surface area and excellent electrical conductivity, could perform as good template for the optimization of HER performance of TMDs.[15−17] Various methods like chemical vapor deposition (CVD),[18] hydrothermal,[19,20] direct ink writing[21] and ascorbic reduction[22] have been employed to manufacture graphene-based aerogels. However, these methods either require template with hard accessibility or could achieve aerogels in which graphene sheets

Received: April 17, 2017
Revised: June 19, 2017
Published: July 2, 2017

ACS Publications © 2017 American Chemical Society

DOI: 10.1021/acssuschemeng.7b01181
ACS Sustainable Chem. Eng. 2017, 5, 6994−7002

Scheme 1. Schematic Illustration for the Preparation of GCA-$MoSe_2$ Hybrid

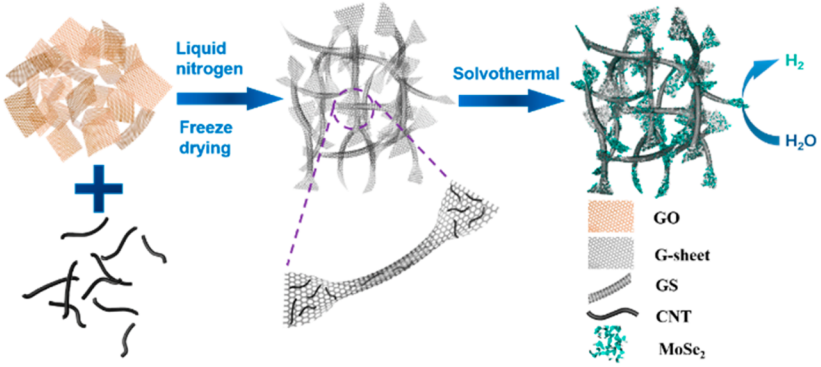

usually stack to form thick slabs between the macropores, leaving behind inner layers inaccessible to electrolyte. Other carbon nanomaterials like one-dimensional carbon nanotubes (CNTs) have been previously introduced to act as spacers to prevent graphene from restacking.[23,24] Incorporation of CNTs into aerogel can space the graphene layers with additional mesopores to allow more complete impregnation of electrolyte, thus improving the electrochemical performance.[25] Recently, graphene scrolls have been reported to be prepared by rolling graphene sheets, with enhanced physicochemical properties.[26,27] Graphene scrolls display similar tubular structure as CNTs, but have open edges, and the interlayer spaces can be easily intercalated. When introduced to assemble with graphene sheets, graphene scrolls could exert the structural advantages and prevent the restacking of the unscrolled sheets.[28]

In this work, we demonstrate a shock cooling method using liquid nitrogen to prepare graphene-CNT aerogel (GCA), and after subsequent lyophilization and carbonization, a unique scroll-sheet conjoined structure is achieved due to partially rolling and template-free assembly of graphene layers. The incorporation of CNTs into the graphene backbone could alleviate the restacking of graphene layers and further enhance the conductivity of the whole structure. By a solvothermal process, $MoSe_2$ nanosheets are vertically immobilized on the all-carbon framework, fully exposing abundant active edge sites to the electrolyte while the underlying GCA could facilitate the ion/electron transport. The resultant GCA-$MoSe_2$ hybrid could be used as an efficient electrocatalyst for HER. The performance was measured by liner sweep voltammetry (LSV) curves and cycling test was also conducted to verify its stability in acidic media.

EXPERIMENTAL SECTION

Materials. Multiwalled carbon nanotubes (MWCNTs) (diameter = 30−50 nm) were obtained from Chengdu Organic Chemicals Co., Ltd., synthesized by the CVD method. H_2SO_4 (95−98%), H_2O_2 (30%), HNO_3 (65%), *N*,*N*-dimethylformamide (DMF, ≥99.5%), ethanol, glucose, potassium permanganate ($KMnO_4$), sodium molybdate dihydrate (Na_2MoO_4) (99.99%), selenium (Se) powder, and hydrazine hydrate ($N_2H_4{\cdot}H_2O$, 50 wt % in water) were purchased from Sinopham Chemical Reagent Co., Ltd. Natural graphite powder (325 mesh) was purchased from Alfa-Aesar (Ward Hill, MA) and used without further purification. Deionized (DI) water was used throughout the experiments. All chemicals were analytic grade and used without further purification.

Preparation of Graphene−Carbon Nanotube Aerogel (GCA). Graphite oxide was dispersed in DI water with sonication to form 8 mg mL^{-1} graphene oxide (GO) dispersion. CNTs were acidized by the mixture of HNO_3/H_2SO_4 (volume ratio = 1:3) at 70 °C for 2 h, and then dispersed in DI water to form 4 mg mL^{-1} dispersion. The above two dispersions of GO and CNTs were mixed together under vigorous stirring with volume ratio of 1:1 and poured into 7 mL centrifuge tube. The centrifuge tube was immersed into liquid nitrogen and the dispersion was frozen rapidly by the shock cooling. After subsequent lyophilization, GO−CNT aerogel (GOCA) was obtained and then placed in a tubular furnace for carbonization under nitrogen flow at 800 °C for 2 h with a heating rate of 5 °C min^{-1}. After naturally cooling down to room temperature, GCA was obtained.

Preparation of GCA-$MoSe_2$ Hybrids. The synthetic procedure of GCA-$MoSe_2$ hybrid by a one-pot solvothermal reaction method is illustrated in Scheme 1. 150 mg of selenium (Se) powder was dispersed in 50 mL of hydrazine hydrate via vigorous stirring to obtain 3 mg mL^{-1} Se dispersion and then heated at 80 °C for 1 h. A certain amount of Na_2MoO_4 was added into 15 mL DMF, and Se dispersion was dropwise added into the above DMF solution with a Mo/Se molar ratio of 1:2. GCA was sliced into pieces with mass of 10 mg and immersed into the precursor solution, followed by transferring to 40 mL Teflon autoclave and reacting at 180 °C for 12 h. Afterward, the as-obtained GCA-$MoSe_2$ hybrid was collected and washed with DI water for several times. After freeze-drying, the final product was obtained by annealing at 450 °C for 2 h with a ramping rate of 5 °C min^{-1} to increase the crystallinity of $MoSe_2$ nanosheets. To achieve GCA-$MoSe_2$ hybrids with different loading of $MoSe_2$, 15, 30, and 60 mg of Se were added respectively, and the corresponding final products were denoted as GCA-$MoSe_2$-1, GCA-$MoSe_2$-2, and GCA-$MoSe_2$-3.

For comparison, pure $MoSe_2$ was prepared without adding GCA to the precursor solution. Graphene aerogel−$MoSe_2$ (GA-$MoSe_2$) hybrid was prepared by using GA to substitute GCA as supporting material, which was prepared by shock cooling of neat GO dispersion (4 mg mL^{-1}) using liquid nitrogen.

Characterization. Raman spectra were performed on a JobinYvon XploRA Raman spectrometer at an exciting wavelength of 632.8 nm. The morphology of samples was characterized by field emission scanning microscopy (FESEM) (Ultra 55, Zesis) at an acceleration voltage of 5 kV, and the chemical composition was studied by energy dispersive X-ray spectroscopy (EDX). Transmission electron microscopy (TEM) observations were conducted by JEOL JEM 2100 TEM under an acceleration voltage of 200 kV. Samples for TEM observations were prepared by dropping solution on the copper grids followed by drying. The crystalline structure was characterized by X-ray diffraction (XRD) conducted on an X'Pert Pro X-ray diffractometer with Cu Kα radiation (λ = 0.1542 nm) under a current of 40 mA and a voltage of 40 kV with 2θ ranges from 5° to 80°. X-ray photoelectron spectroscopy (XPS) analysis was performed with a VG ESCALAB 220I-XL device and all XPS spectra were corrected using C 1s line at 284.5 eV. In addition, the curve fitting and background subtraction were accomplished using XPS PEAK41 software.

Electrochemical Measurements. Prior to all the hydrogen evolution experiments, glassy carbon electrodes (GCE) (diameter = 3 mm) were pretreated according to the previous report.[29] The working electrode was prepared as follows: 2 mg of GCA-$MoSe_2$ hybrid was

DOI: 10.1021/acssuschemeng.7b01181
ACS Sustainable Chem. Eng. 2017, 5, 6994−7002

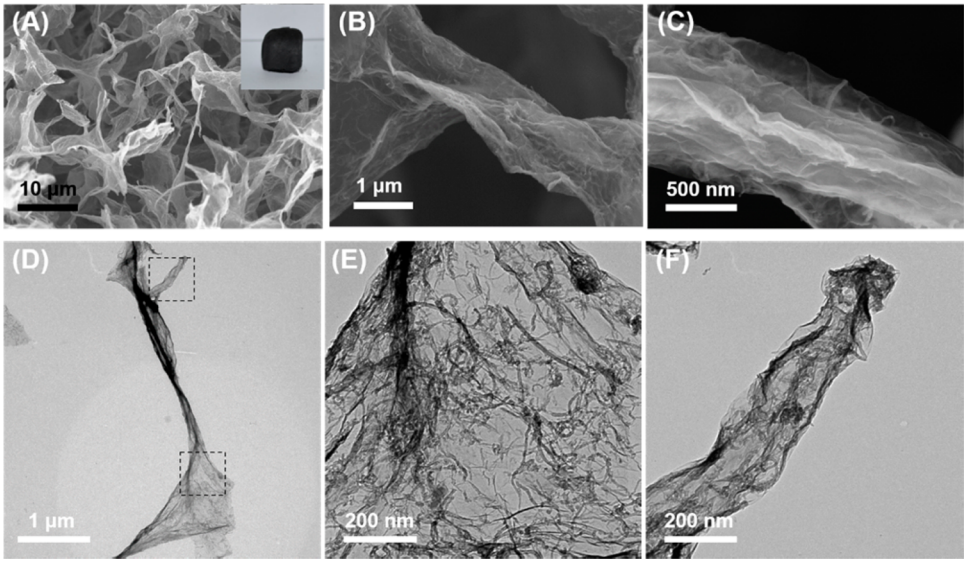

Figure 1. (A) SEM image of the incorporated graphene scroll-sheet conjoined structure in GCA, and the amplified image (B) of CNTs-graphene sheet, and (C) CNTs-graphene scroll. Inset is the digital image of GCA. TEM image (D) of CNT incorporated graphene scroll-sheet conjoined structure, and the high magnification images of selected area of (E) CNTs-graphene sheet and (F) CNTs-graphene scroll.

dispersed in 1 mL DMF/DI water mixed solution (volume ratio = 2:1) containing 20 μL 5 wt % Nafion. After being sonicated for 2 h, 8 μL of the as-obtained slurry was dropped onto GCE and dried at room temperature to achieve GCA-$MoSe_2$ hybrid modified GCE.

All electrochemical tests were performed in a standard three-electrode setup using CHI 660D electrochemical workstation (Chenhua Instruments Co, Shanghai, China) at room temperature, where sample modified GCE was applied as the working electrode, saturated calomel electrode (SCE) as the reference electrode and graphite rod as counter electrode. The electrocatalysis of samples toward HER was carried out by liner sweep voltammetry (LSV) in nitrogen purged 0.5 M H_2SO_4 with scan rate of 2 mV s^{-1}. Electrochemical Impedance spectroscopy (EIS) measurements were conducted in 0.5 M H_2SO_4 from 0.01 to 100 Hz at a potential of 200 mV vs RHE with the amplitude of 5 mV. The cycling stability was investigated by cyclic voltammetry (CV) between −0.35 and 0.25 V vs RHE at a scan rate of 100 mV s^{-1}. In all electrochemical tests, the potentials were calibrated to RHE according to the equation of $E_{RHE} = E_{SCE} + (0.241 + 0.059\ pH)$ V.

RESULTS AND DISCUSSION

Morphology and Structure of GCA-$MoSe_2$ Hybrids. GOCA was fabricated by direct shock cooling of the GO/CNT mixed aqueous dispersion. However, pure CNTs could not self-assemble to form aerogel by the same shock cooling procedure. Only when GO was added as cross-linking agent, the aerogel could form and be shaped up by the vessel. The as-obtained GOCA displays black color, which is distinctly different from the brown color of GO aerogel prepared in the absence of CNTs (Figure S1A). The inner structure of GCA is a 3D network conjoined by graphene scrolls and sheets (Figure 1A). This unique morphology is induced by the shock cooling effect of liquid nitrogen. In this process, the shrinkage of graphene layers occurs and drive flat GO sheets to roll up into scrolls, which is a more energetically favorable state. These scrolls assemble with adjacent layers to form a 3D network. The calcination in the final step can reduce GO to graphene, as well as remove the oxygen containing groups in CNTs, while the scroll-sheet conjoined network could be well retained. In the microscopic structure, the existence of scrolls can prohibit graphene sheets from severely restacking, and lead to generation of macropores. CNTs coexist with graphene in two forms: intercalating between the graphene sheets (Figure 1B) or being enwrapped by the tubular graphene scrolls (Figure 1C). TEM images further reveal that the thin graphene layers are partially rolled to form the unique scroll-sheet conjoining structure (Figure 1D). CNTs were observed to interconnect with each other and evenly adhere to graphene wall in both cases (Figure 1E and 1F). The uniform hybridization of graphene and CNTs is derived from the homogeneous dispersion of GO and CNTs through the $\pi-\pi$ interactions in precursor dispersion. The GOCA was converted into GCA by the high temperature calcination. From the Raman spectra presented in Figure S1B, G band and D band were observed for both GOCA and GCA. For GOCA, the intensity ratio of D band (I_D) to G band (I_G) is 0.99, and the value is estimated to be 1.04 for GOCA, evidencing the reduction of GO by calcination. In addition, the all-carbon framework shows a nearly complete recovery after more than 50% compression as 1800 times of its bulk weight is imposed on (Figure S1C). This high compressibility can be attributed to the reinforcement of incorporated CNTs on relatively flexible graphene, which endow the scroll-sheet conjoined structure with intrinsic elasticity and elastic buckling under pressure. Furthermore, either attaching on the graphene sheets or being enwrapped by the graphene scrolls, the CNTs intertwining with each other could enhance the conductivity (5 S m^{-1} for GA, 12 S m^{-1} for GCA) and provide faster electron transfer pathway. The insertion or intercalation of CNTs between graphene interlayers can further hinder the restacking of graphene layers in these isolated sheets or scrolls and produce some mesopores. The hierarchical porous structure of CNTs incorporated graphene aerogel could also provide more regions for the growth of $MoSe_2$ nanosheets while the simplicity of this shock cooling method make it accessible for large-scale production.

Without any template for growing, pure $MoSe_2$ tends to form irregular shaped agglomerates with sizes of several micrometers (Figure S2A, S2B). When GCA serves as template for in situ growth of $MoSe_2$, ultrathin vertically oriented nanosheets can be anchored on the carbon skeleton (Figure 2A). With a proper

DOI: 10.1021/acssuschemeng.7b01181
ACS Sustainable Chem. Eng. 2017, 5, 6994−7002

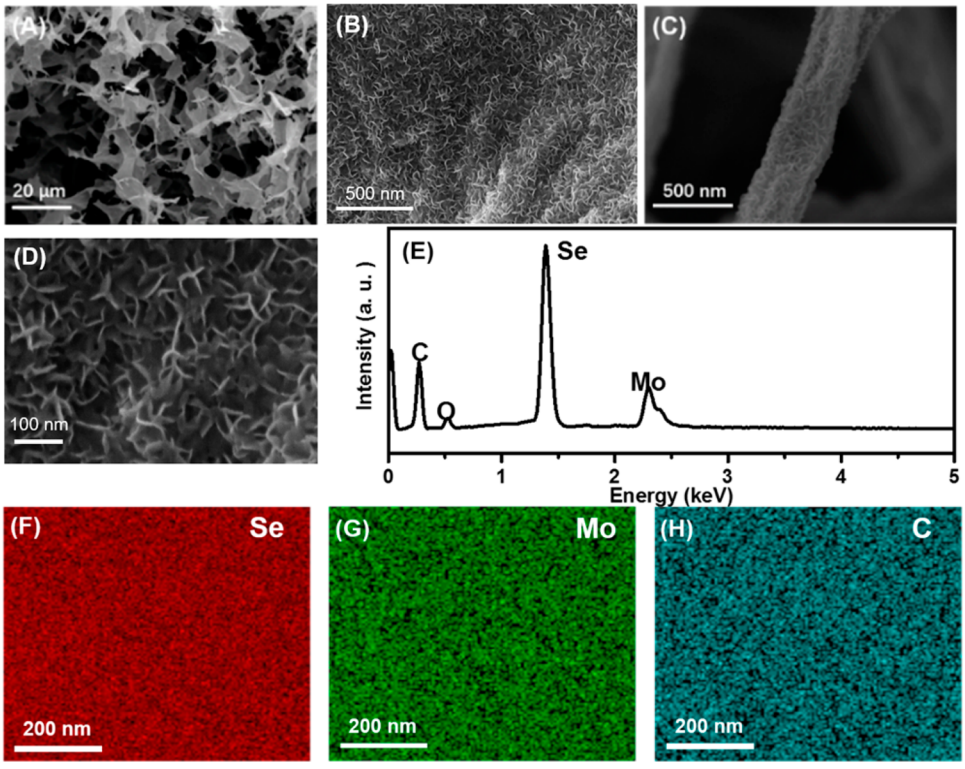

Figure 2. FESEM image of (A) GCA-$MoSe_2$-2, and images of $MoSe_2$ nanosheets grown vertically on (B) graphene sheet and (C) graphene scroll in the aerogel structure, respectively. High magnification FESEM image of (D) GCA-$MoSe_2$-2 and (E) EDX spectrum taken from corresponding area and the elemental mapping for (F) Se, (G) Mo, (H) C.

loading of $MoSe_2$ nanosheets, the robust 3D scroll-sheet conjoined architecture was well retained without any collapse or blocking of the pores. From the high-magnification SEM images in Figure 2B and 2C, it is seen that $MoSe_2$ is uniformly distributed on the graphene scrolls as well as the graphene sheets, maximizing its active edges. The EDX results taken from $MoSe_2$ anchored graphene scrolls could further prove the even distribution of $MoSe_2$ nanosheets on the carbon framework (Figure 2D–H). The atom ratio of Se to Mo evaluated from EDX spectrum is 2.15:1, which is very close to that (2:1) of $MoSe_2$. From the TEM image, it is clearly observed that in the hybrid structure, CNTs tangling with each other are enwrapped by graphene scrolls (Figure 3A), while $MoSe_2$ nanosheets are anchored on the outer wall of graphene scrolls, displaying a few-layered structure (Figure 3B). The interlayer spacing approximates 0.65 nm, which falls into the typical value of layered $MoSe_2$.[30] And the lattice fringe is measured to be 0.28 nm, which corresponds to the (100) face of the $MoSe_2$ crystal.[31]

XRD pattern of pure GCA displays a peak centered at 2θ = 26.4°, which can be assigned to the (002) plane of stacked carbon sheets. For GCA-$MoSe_2$-2 and GA-$MoSe_2$, four other sharp peaks at 2θ = 13.0°, 32.1°, 37.4°, and 56.3° can also be observed and indexed to the (002), (100), (103), and (110) diffraction planes of hexagonal $MoSe_2$, respectively, which is the same as pure $MoSe_2$ (Figure 4). The XRD results confirm the successful anchoring of $MoSe_2$ nanosheets on the supporting material of GCA or GA with good crystallinity after annealing. XPS spectra were measured to study the composition and surface chemical state of GCA-$MoSe_2$. From the survey spectrum of GCA-$MoSe_2$-2, C, Se, and Mo are observed as main elements coexisting in the hybrid (Figure 5A). The high

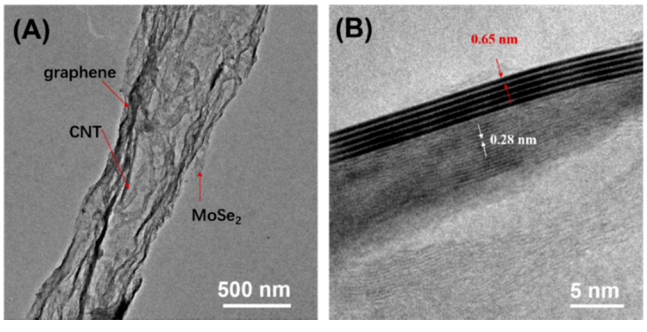

Figure 3. TEM images of GCA-$MoSe_2$-2 at (A) low and (B) high magnifications.

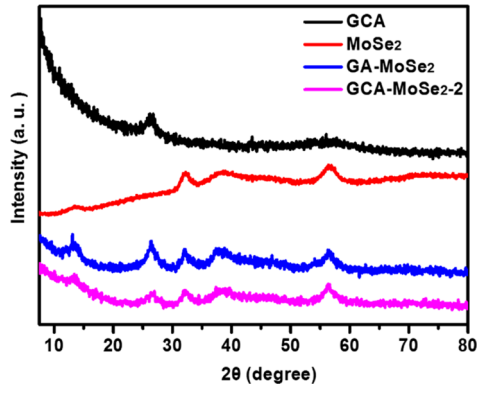

Figure 4. XRD patterns of GCA, pure $MoSe_2$, GCA-$MoSe_2$-2, and GA-$MoSe_2$.

DOI: 10.1021/acssuschemeng.7b01181
ACS Sustainable Chem. Eng. 2017, 5, 6994–7002

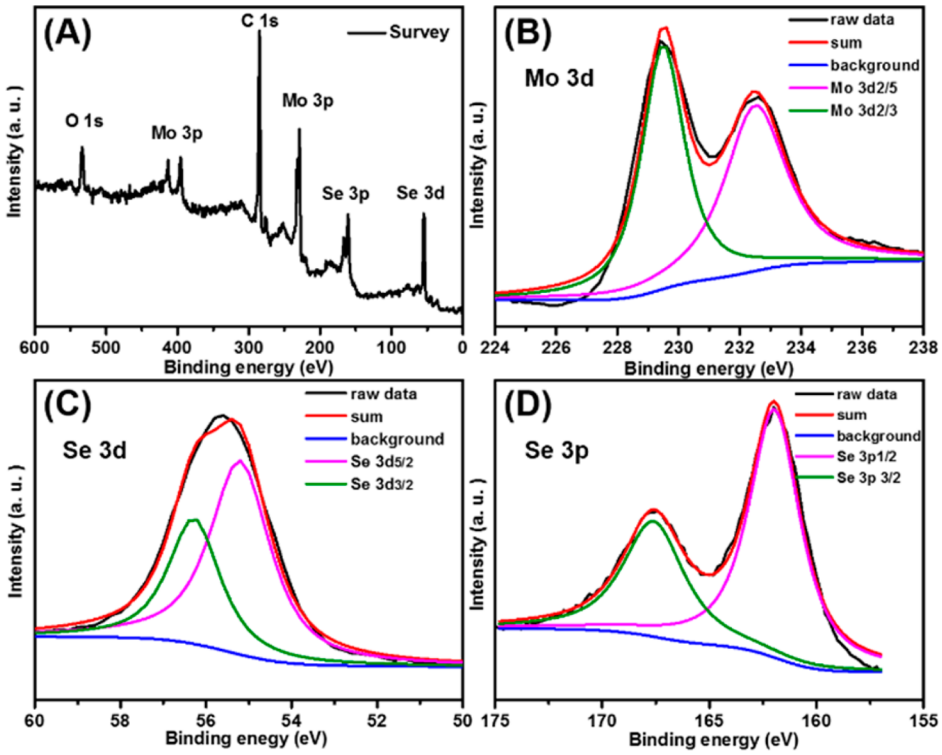

Figure 5. (A) XPS survey spectrum and high resolution (B) Mo 3d spectrum, (C) Se 3d spectrum, and (D) Se 3p spectrum of GCA-$MoSe_2$-2.

resolution Mo 3d spectrum can be deconvoluted into two peaks centered at 229.5 and 232.6 eV, which belong to Mo $3d_{5/2}$ and Mo $3d_{3/2}$, respectively, revealing the chemical state of Mo^{4+} in GCA-$MoSe_2$-2 (Figure 5B).[32] The high resolution spectrum of Se 3d shows two peaks of Se $3d_{3/2}$ and Se $3d_{5/2}$, with the binding energy at 56.3 and 55.0 eV (Figure 5C), while the spectrum of Se 3p can be deconvoluted into peaks at 162.0 and 167.6 eV, which could be attributed to Se $3p_{1/2}$ and Se $3p_{3/2}$ (Figure 5D), all indicating the valence state of −2 for Se in the hybrid.[14]

Electrocatalytic Activity of GCA-$MoSe_2$ toward HER. The electrocatalytic activities of GCA-$MoSe_2$ hybrids toward HER were investigated using a three-electrode setup in the electrolyte of 0.5 M H_2SO_4. LSV curves of GCA, pure $MoSe_2$, GCA-$MoSe_2$-2, and GA-$MoSe_2$ were all measured and presented in Figure 6A. GCA displays no catalytic activity toward HER as its LSV curve almost approaches a horizontal line. Pure $MoSe_2$, GCA-$MoSe_2$, and GA-$MoSe_2$ all show distinct catalytic activity according to their LSV curves, indicating $MoSe_2$ is the core catalytic material in the hybrid. For bulk $MoSe_2$, the tendency of aggregation hinders the electrocatalytic activity. When GCA serves as support for anchoring $MoSe_2$ nanosheets, the HER performance can be dramatically promoted, which is manifested by a shift of onset potential from 198 mV to 113 mV, and less energy for driving a current density of 10 mA cm^{-2} (an overpotential of 297 mV for $MoSe_2$ while only 228 mV for GCA-$MoSe_2$). As the basal edges of $MoSe_2$ have been identified as catalytic active sites for HER, the perpendicularly grown $MoSe_2$ nanosheets could not only maximize the active sites, but also facilitate ion/electrolyte transport at the electrode interface. The all-carbon aerogel performing as supporting material could minimize the aggregation and restacking of the $MoSe_2$ nanosheets, and also improve the electrical contact between electrocatalyst and the electrode with its intrinsic scroll-sheet conjoining conductive network. The graphene scrolls interconnect graphene sheets, inhibiting them from restacking, thus exposing more surface area for anchoring $MoSe_2$ nanosheets. Furthermore, this scroll-sheet conjoining structure could leave macropores in the hybrid, enabling full impregnation of electrolyte, thus improving the HER catalytic behavior. The improved electrochemical active surface area (ECSA) of GCA-$MoSe_2$ is further confirmed by the double layer capacitance (C_{dl}). C_{dl} was measured by cyclic voltammetry (Figure 6C, 6D) in the potential range with no faradaic response for both GCA-$MoSe_2$-2 and pure $MoSe_2$. The C_{dl} of GCA-$MoSe_2$-2 is estimated to be 1.31 mF cm^{-2}, which is more than 2-fold of that of pure $MoSe_2$ (0.51 mF cm^{-2}), indicating that the ECSA of GCA-$MoSe_2$-2 is greatly enhanced compared with pure $MoSe_2$ (Figure S3A, S3B). It is worth noting that GCA-$MoSe_2$-2 shows superior HER catalytic performance than GA-$MoSe_2$ as the latter shows higher onset potential and lower current density at the same overpotential. Evidently, the great difference of the HER performance between the two hybrids is caused by the incorporation of CNTs into the graphene scroll-sheet conjoined network. CNTs, displaying a 1D tubular structure,[33] could enable a more accessible electrolyte contact by the spacing effect and enhance the conductivity by shortening the electron transport pathway, contributing to improved HER performance.[34,35]

The loading amount of $MoSe_2$, which is controllable by tuning the addition amount of Se and Na_2MoO_4, also has a great influence on the HER electrocatalytic activity of GCA-$MoSe_2$. As indicated by the LSV curves in Figure S4, among all the three samples, GCA-$MoSe_2$-2, presents the most outstanding HER electrocatalytic activity since it displays a more positive onset potential and higher current density at the same overpotential in the LSV curve than the other two. GCA-$MoSe_2$-2 displays a well-defined hierarchical structure where few-layered $MoSe_2$ nanosheets are vertically grown on scroll-

DOI: 10.1021/acssuschemeng.7b01181
ACS Sustainable Chem. Eng. 2017, 5, 6994−7002

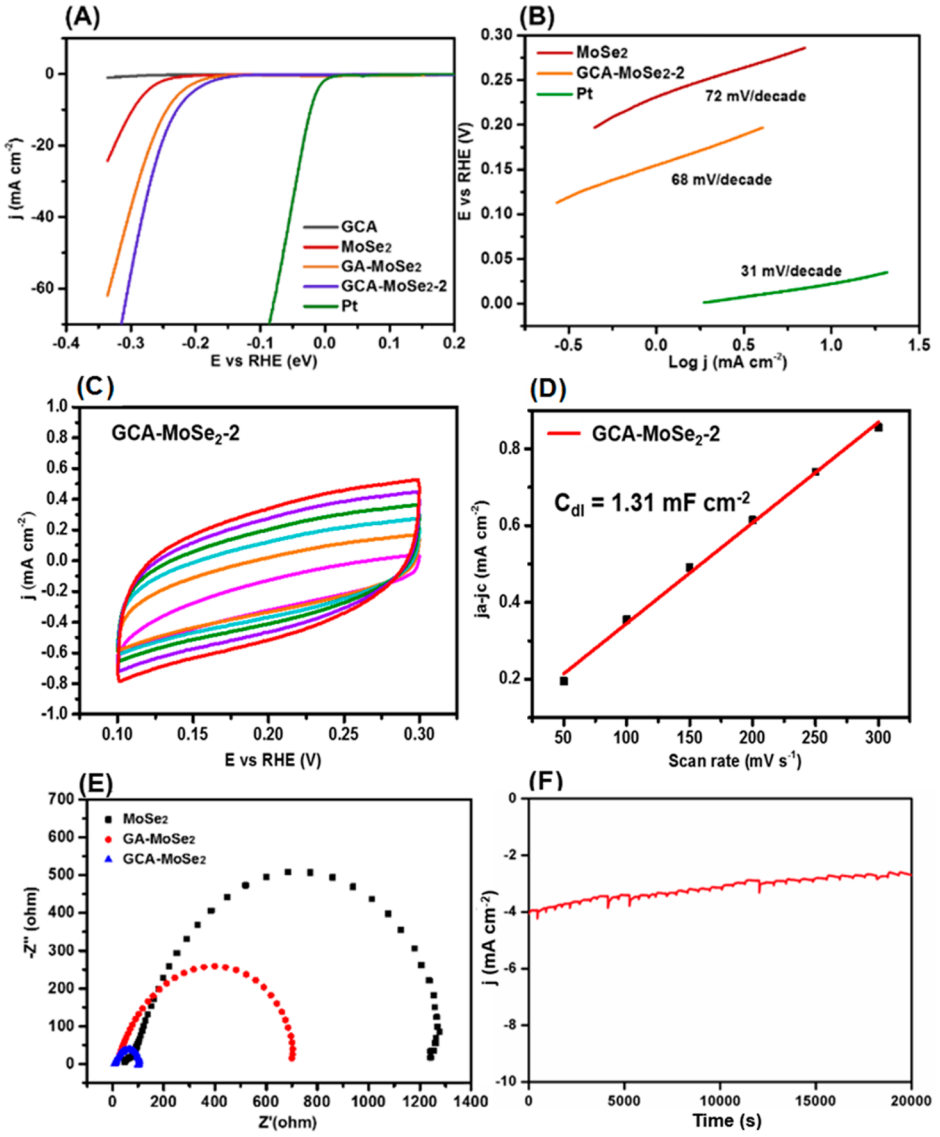

Figure 6. (A) LSV polarization curves for GCA, $MoSe_2$, GA-$MoSe_2$, and GCA-$MoSe_2$-2 modified GCE in N_2-purged 0.5 M H_2SO_4 solution. Scan rate: 2 mV s^{-1}. (B) Tafel plots for pure $MoSe_2$, GCA-$MoSe_2$, and Pt modified GCE. (C) CV curves of GCA-MoSe2-2 in the region of 0.1−0.3 V vs RHE at scan rate of 50, 100, 150, 200, 250, 300 mV s^{-1}. (D) Plot showing the extraction of the double layer capacitance (C_{dl}) of GCA-$MoSe_2$-2 at 0.2 V vs RHE. (E) Nyquist plots for $MoSe_2$, GCA-$MoSe_2$ and GA-$MoSe_2$ at a potential of −200 mV vs RHE. (F) i−t curve for GA-$MoSe_2$-2 modified GCE.

sheet conjoined skeleton with a fine coverage, maximizing the exposed catalytic active sites. For GCA-$MoSe_2$-1 prepared with 15 mg of Se, $MoSe_2$ nanosheets with smaller size were sparsely immobilized on the GCA, and the embossing sketch of CNTs attached on graphene surface beneath the thin coverage of $MoSe_2$ could even be observed (Figure S5A, S5B). The less loading amount of $MoSe_2$ results in less active edges being exposed for electrocatalysis. While for GCA-$MoSe_2$-3, the overloading of $MoSe_2$ causes severe aggregation, leading to loss of active edges. Furthermore, the overgrowth of $MoSe_2$ nanosheets goes toward the pore regions, causing the breaking of the porous structure (Figure S5C, S5D). Therefore, proper loading of $MoSe_2$ on the carbon support could render optimized HER catalytic performance for GCA-$MoSe_2$-2.

Tafel plots are extracted from the LSV curves for quantitative analysis of HER performance of different samples as shown in Figure 6B. The Tafel plots are well fitted to the Tafel equation, $\eta = b \log(j) + a$, where η is the overpotential, j is the current density, and b is the Tafel slope. For pure $MoSe_2$, GCA-$MoSe_2$-2, and Pt, the Tafel slope is calculated to be 72, 68, and 31 mV $decade^{-1}$, respectively. The decreased Tafel slope of GCA-$MoSe_2$-2 compared with pure $MoSe_2$ suggests less activation energy for electrocatalytic reaction, which can be ascribed to the confined growth of $MoSe_2$ nanosheets onto GCA so that perpendicularly oriented, uniformly distributed and thereby edge-rich morphologies are formed for the GCA-$MoSe_2$-2 hybrid. The Tafel slope of 68 mV $decade^{-1}$ for GCA-$MoSe_2$-2 suggests that HER proceeds by a Volmer-Heyrovsky mechanism where a rapid discharge step (the Volmer reaction) comes first and a rate-limiting electrochemical desorption step (the Heyrovsky reaction) follows up. The catalytic performance of GCA-$MoSe_2$-2 prepared by us is comparable or superior to other previous reported $MoSe_2$ based electrocatalysts (Table 1). This result further highlights the important role of GCA as template for anchoring $MoSe_2$ nanosheets and enabling abundant active edges being exposed to the electrolyte. This

DOI: 10.1021/acssuschemeng.7b01181
ACS Sustainable Chem. Eng. 2017, 5, 6994−7002

Table 1. Comparison of the HER Performance of Different $MoSe_2$-Based Catalysts

catalyst	j (mA cm^{-2})	E vs RHE (V)	Tafel slope (mV dec^{-1})	ref
$MoSe_{2-x}$	13.4	0.300	98	36
$MoSe_2$/GCD	10	0.290	101	37
$MoSe_2$ film			105−120	38
$MoSe_2$-PCF	10	0.230	62	39
$MoSe_2$/$CoSe_2$	90.4	0.350	73	40
Exf-$MoSe_2$	0	0.350	82	41
GCA-$MoSe_2$-1	10	0.247	72	this work
GCA-$MoSe_2$-2	10	0.228	68	this work
GCA-$MoSe_2$-3	10	0.252	71	this work

facilely fabricated all carbon scroll-sheet conjoined 3D skeleton derived from graphene-CNTs hybrids demonstrates its unique advantage by offering a fast electron transfer pathway which is beneficial to the electrocatalytic activity.

EIS tests were conducted for pure $MoSe_2$, GCA-$MoSe_2$, and GA-$MoSe_2$. The Nyquist plots indicate that GCA-$MoSe_2$ has smaller charge transfer resistance (R_{ct}) of 100 Ω, than those of pure $MoSe_2$ and GA-$MoSe_2$ (Figure 6E). The EIS results supply to verify the enhanced Faradaic process and thus improved HER kinetics of the hybrid by coupling $MoSe_2$ with GCA. The durability of GCA-$MoSe_2$ hybrid is investigated via carrying out continuous electrocatalytic HER performance at a constant overpotential (Figure 6F). It can be observed that the current density exhibits only a slight attenuation after cycling for 20000 s, revealing the long-term stability of GCA-$MoSe_2$ electrocatalyst. The fluctuation of the curve is mainly due to the alternate accumulation and release processes of produced H_2 (g) bubbles that occur fiercely on the surface of the electrode material, indicating the rapid depletion of H^+ in electrolyte, which may result in the degradation in current density. The LSV curve of GCA-$MoSe_2$ hybrid almost overlaps with the initial one after continuously 3000 CV cycles, with only very slight left shift, further confirming that the catalyst is highly stable (Figure 7A). The good stability of GCA-$MoSe_2$ electrocatalyst can be attributed to its robust morphology that keeps well during the violent hydrogen evolution reaction (Figure 7B).

CONCLUSIONS

In conclusion, GCA with unique scroll-sheet conjoined structure has been prepared via a simple liquid nitrogen shock cooling method. The as-obtained GCA exhibiting porous microscopic structure as well as macroscopic elasticity was used as substrate for the immobilization of $MoSe_2$ nanosheets through a solvothermal procedure. The hierarchically structured GCA-$MoSe_2$ with proper and uniform loading of $MoSe_2$ nanosheets on the all-carbon skeleton can render abundant active sites exposed to the electrolyte for catalyzing HER process. The unique CNTs incorporated scroll-sheet conjoined graphene aerogel also enables full impregnation of electrolyte into the electrode material and affords high conductivity for ion diffusion and electron transfer. The ensemble of these properties makes GCA-$MoSe_2$ hybrid potential candidate for HER electrocatalysis. The facilely prepared and well-designed GCA could be extended to immobilize other guest materials for a vast variety of applications.

ASSOCIATED CONTENT

Supporting Information

The Supporting Information is available free of charge on the ACS Publications website at DOI: 10.1021/acssuschemeng.7b01181.

Digital image of GA, GCA, and CNTs and corresponding Raman spectrum; FESEM images of pure $MoSe_2$, GCA-$MoSe_2$-1, and GCA-$MoSe_2$-3; ECSA evaluation; LSV polarization curves for different GCA-$MoSe_2$ samples (PDF)

AUTHOR INFORMATION

Corresponding Authors

*E-mail: weifan@dhu.edu.cn.

*Email: txliu@fudan.edu.cn or txliu@dhu.edu.cn. Tel: +86-21-55664197. Fax: +86-21-65640293.

ORCID

Wei Fan: 0000-0001-6978-1405

Tianxi Liu: 0000-0002-5592-7386

Notes

The authors declare no competing financial interest.

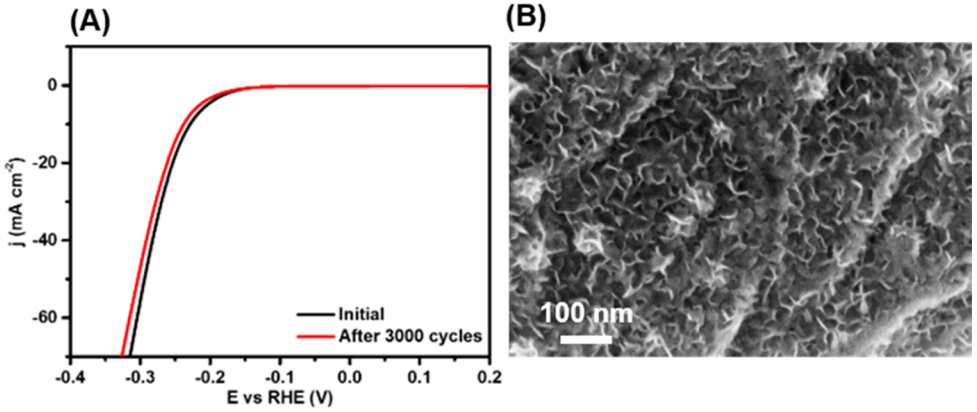

Figure 7. (A) LSV polarization curves for GA-$MoSe_2$-2 modified GCE recorded before and after 3000 times of CV cycle. (B) SEM image of GA-$MoSe_2$-2 after cycling test.

DOI: 10.1021/acssuschemeng.7b01181
ACS Sustainable Chem. Eng. 2017, 5, 6994−7002

■ ACKNOWLEDGMENTS

The authors are grateful for the financial support from the National Natural Science Foundation of China (51433001, 21674019), China Postdoctoral Science Foundation (2016M601471), Shanghai Sailing Program (17YF1400200), and the Fundamental Research Funds for the Central Universities.

■ REFERENCES

(1) Zou, X.; Zhang, Y. Noble Metal-free hydrogen evolution catalysts for water splitting. *Chem. Soc. Rev.* **2015**, *44* (15), 5148−5180.
(2) Kong, D.; Cha, J. J.; Wang, H.; Lee, H. R.; Cui, Y. First-row transition metal dichalcogenide catalysts for hydrogen evolution reaction. *Energy Environ. Sci.* **2013**, *6* (12), 3553−3558.
(3) Chhowalla, M.; Shin, H. S.; Eda, G.; Li, L.-J.; Loh, K. P.; Zhang, H. The chemistry of two-dimensional layered transition metal dichalcogenide nanosheets. *Nat. Chem.* **2013**, *5* (4), 263−275.
(4) Li, Y.; Wang, H.; Xie, L.; Liang, Y.; Hong, G.; Dai, H. MoS_2 nanoparticles grown on graphene: An advanced catalyst for the hydrogen evolution reaction. *J. Am. Chem. Soc.* **2011**, *133* (19), 7296−7299.
(5) Voiry, D.; Yamaguchi, H.; Li, J.; Silva, R.; Alves, D. C.; Fujita, T.; Chen, M.; Asefa, T.; Shenoy, V. B.; Eda, G.; Chhowalla, M. Enhanced catalytic activity in strained chemically exfoliated WS_2 nanosheets for hydrogen evolution. *Nat. Mater.* **2013**, *12* (9), 850−855.
(6) Voiry, D.; Yang, J.; Chhowalla, M. Recent strategies for improving the catalytic activity of 2D TMD nanosheets toward the hydrogen evolution reaction. *Adv. Mater.* **2016**, *28*, 6197−6206.
(7) Kibsgaard, J.; Chen, Z.; Reinecke, B. N.; Jaramillo, T. F. Engineering the surface structure of MoS_2 to preferentially expose active edge sites for electrocatalysis. *Nat. Mater.* **2012**, *11* (11), 963−969.
(8) Wang, H.; Kong, D.; Johanes, P.; Cha, J. J.; Zheng, G.; Yan, K.; Liu, N.; Cui, Y. $MoSe_2$ and WSe_2 nanofilms with vertically aligned molecular layers on curved and rough surfaces. *Nano Lett.* **2013**, *13* (7), 3426−3433.
(9) Mao, S.; Wen, Z.; Ci, S.; Guo, X.; Ostrikov, K. K.; Chen, J. Perpendicularly oriented $MoSe_2$/graphene nanosheets as advanced electrocatalysts for hydrogen evolution. *Small* **2015**, *11* (4), 414−419.
(10) Huang, Y.; Lu, H.; Gu, H.; Fu, J.; Mo, S.; Wei, C.; Miao, Y.-E.; Liu, T. A CNT@$MoSe_2$ hybrid catalyst for efficient and stable hydrogen evolution. *Nanoscale* **2015**, *7* (44), 18595−18602.
(11) Liu, Z.; Li, N.; Zhao, H.; Du, Y. Colloidally synthesized $MoSe_2$/graphene hybrid nanostructures as efficient electrocatalysts for hydrogen evolution. *J. Mater. Chem. A* **2015**, *3* (39), 19706−19710.
(12) Xu, S.; Lei, Z.; Wu, P. Facile preparation of 3D MoS_2/$MoSe_2$ nanosheet−graphene networks as efficient electrocatalysts for the hydrogen evolution reaction. *J. Mater. Chem. A* **2015**, *3* (31), 16337−16347.
(13) Liu, Y.; Ren, L.; Zhang, Z.; Qi, X.; Li, H.; Zhong, J. 3D Binder-free $MoSe_2$ nanosheets/carbon cloth electrodes for efficient and stable hydrogen evolution prepared by simple electrophoresis deposition strategy. *Sci. Rep.* **2016**, *6*, 22516.
(14) Zhang, Y.; Zuo, L.; Zhang, L.; Huang, Y.; Lu, H.; Fan, W.; Liu, T. Cotton wool derived carbon fiber aerogel supported few-layered $MoSe_2$ nanosheets as efficient electrocatalysts for hydrogen evolution. *ACS Appl. Mater. Interfaces* **2016**, *8* (11), 7077−7085.
(15) Zhao, Y.; Xie, X.; Zhang, J.; Liu, H.; Ahn, H. J.; Sun, K.; Wang, G. MoS_2 nanosheets supported on 3D graphene aerogel as a highly efficient catalyst for hydrogen evolution. *Chem. - Eur. J.* **2015**, *21* (45), 15908−15913.
(16) Hou, Y.; Zhang, B.; Wen, Z.; Cui, S.; Guo, X.; He, Z.; Chen, J. A 3D hybrid of layered MoS_2/nitrogen-doped graphene nanosheet aerogels: an effective catalyst for hydrogen evolution in microbial electrolysis cells. *J. Mater. Chem. A* **2014**, *2* (34), 13795−13800.
(17) Worsley, M. A.; Shin, S. J.; Merrill, M. D.; Lenhardt, J.; Nelson, A. J.; Woo, L. Y.; Gash, A. E.; Baumann, T. F.; Orme, C. A. Ultralow density, monolithic WS_2, MoS_2, and MoS_2/graphene aerogels. *ACS Nano* **2015**, *9* (5), 4698−4705.
(18) Min, B. H.; Kim, D. W.; Kim, K. H.; Choi, H. O.; Jang, S. W.; Jung, H.-T. Bulk scale growth of CVD graphene on Ni nanowire foams for a highly dense and elastic 3D conducting electrode. *Carbon* **2014**, *80*, 446−452.
(19) Lv, P.; Tan, X.-W.; Yu, K.-H.; Zheng, R.-L.; Zheng, J.-J.; Wei, W. Super-elastic graphene/carbon nanotube aerogel: A novel thermal interface material with highly thermal transport properties. *Carbon* **2016**, *99*, 222−228.
(20) Li, Y.; Chen, J.; Huang, L.; Li, C.; Hong, J. D.; Shi, G. Highly compressible macroporous graphene monoliths via an improved hydrothermal process. *Adv. Mater.* **2014**, *26* (28), 4789−4793.
(21) Zhu, C.; Han, T. Y.-J.; Duoss, E. B.; Golobic, A. M.; Kuntz, J. D.; Spadaccini, C. M.; Worsley, M. A. Highly compressible 3D periodic graphene aerogel microlattices. *Nat. Commun.* **2015**, *6*, 6962.
(22) Qiu, L.; Liu, J. Z.; Chang, S. L. Y.; Wu, Y.; Li, D. Biomimetic superelastic graphene-based cellular monoliths. *Nat. Commun.* **2012**, *3*, 1241.
(23) Yang, S.-Y.; Chang, K.-H.; Tien, H.-W.; Lee, Y.-F.; Li, S.-M.; Wang, Y.-S.; Wang, J.-Y.; Ma, C.-C. M.; Hu, C.-C. Design and tailoring of a hierarchical graphene-carbon nanotube architecture for supercapacitors. *J. Mater. Chem.* **2011**, *21* (7), 2374−2380.
(24) Zhang, C.; Ren, L.; Wang, X.; Liu, T. Graphene oxide-assisted dispersion of pristine multiwalled carbon nanotubes in aqueous media. *J. Phys. Chem. C* **2010**, *114* (26), 11435−11440.
(25) Shao, Q.; Tang, J.; Lin, Y.; Li, J.; Qin, F.; Yuan, J.; Qin, L.-C. Carbon nanotube spaced graphene aerogels with enhanced capacitance in aqueous and ionic liquid electrolytes. *J. Power Sources* **2015**, *278*, 751−759.
(26) Xu, Z.; Zheng, B.; Chen, J.; Gao, C. Highly efficient synthesis of neat graphene nanoscrolls from graphene oxide by well-controlled lyophilization. *Chem. Mater.* **2014**, *26* (23), 6811−6818.
(27) Zheng, B.; Xu, Z.; Gao, C. Mass production of graphene nanoscrolls and their application in high rate performance supercapacitors. *Nanoscale* **2016**, *8* (3), 1413−1420.
(28) Pan, Y.; Zeng, F.; Huang, Z.; Zhou, H.; Kuang, Y. A simple microexplosion synthesis of graphene-based scroll-sheet conjoined nanomaterials for enhanced supercapacitor properties. *Electrochim. Acta* **2015**, *172*, 71−76.
(29) Huang, Y.; Miao, Y.-E.; Zhang, L.; Tjiu, W. W.; Pan, J.; Liu, T. Synthesis of few-layered MoS_2 nanosheet-coated electrospun SnO_2 nanotube heterostructures for enhanced hydrogen evolution reaction. *Nanoscale* **2014**, *6* (18), 10673−10679.
(30) Lee, L. T. L.; He, J.; Wang, B.; Ma, Y.; Wong, K. Y.; Li, Q.; Xiao, X.; Chen, T. Few-layer $MoSe_2$ possessing high catalytic activity towards iodide/tri-iodide redox shuttles. *Sci. Rep.* **2015**, *4*, 4063.
(31) Xia, J.; Huang, X.; Liu, L.-Z.; Wang, M.; Wang, L.; Huang, B.; Zhu, D.-D.; Li, J.-J.; Gu, C.-Z.; Meng, X.-M. CVD synthesis of large-area, highly crystalline $MoSe_2$ atomic layers on diverse substrates and application to photodetectors. *Nanoscale* **2014**, *6* (15), 8949−8955.
(32) Lei, Z.; Xu, S.; Wu, P. Ultra-thin and porous $MoSe_2$ nanosheets: Facile preparation and enhanced electrocatalytic activity towards the hydrogen evolution reaction. *Phys. Chem. Chem. Phys.* **2016**, *18* (1), 70−74.
(33) Li, Y.-X.; Gao, Y.; Yang, C.; Wang, Z.-Q.; Xue, G. Facile and controllable assembly of multiwalled carbon nanotubes on polystyrene microspheres. *Chin. J. Polym. Sci.* **2014**, *32* (6), 711−717.
(34) Youn, D. H.; Han, S.; Kim, J. Y.; Kim, J. Y.; Park, H.; Choi, S. H.; Lee, J. S. Highly active and stable hydrogen evolution electrocatalysts based on molybdenum compounds on carbon nanotube−graphene hybrid support. *ACS Nano* **2014**, *8* (5), 5164−5173.
(35) Peng, S.; Li, L.; Han, X.; Sun, W.; Srinivasan, M.; Mhaisalkar, S. G.; Cheng, F.; Yan, Q.; Chen, J.; Ramakrishna, S. Cobalt sulfide nanosheet/graphene/carbon nanotube nanocomposites as flexible electrodes for hydrogen evolution. *Angew. Chem.* **2014**, *126* (46), 12802−12807.

DOI: 10.1021/acssuschemeng.7b01181
ACS Sustainable Chem. Eng. 2017, 5, 6994−7002

(36) Zhou, X. L.; Jiang, J.; Ding, T.; Zhang, J. J.; Pan, B. C.; Zuo, J.; Yang, Q. Fast colloidal synthesis of scalable Mo-rich hierarchical ultrathin $MoSe_{2-x}$ nanosheets for high-performance hydrogen evolution. *Nanoscale* **2014**, *6* (19), 11046−11051.
(37) Tang, H.; Dou, K.; Kaun, C.-C.; Kuang, Q.; Yang, S. $MoSe_2$ nanosheets and their graphene hybrids: synthesis, characterization and hydrogen evolution reaction studies. *J. Mater. Chem. A* **2014**, *2* (2), 360−364.
(38) Kong, D.; Wang, H.; Cha, J. J.; Pasta, M.; Koski, K. J.; Yao, J.; Cui, Y. Synthesis of MoS_2 and $MoSe_2$ films with vertically aligned layers. *Nano Lett.* **2013**, *13* (3), 1341−1347.
(39) Yan, J.; Zhang, Y.; Huang, Y.; Miao, Y. E.; Liu, T. $MoSe_2$ nanosheets grown on polydopamine-derived porous fibers: a high-performance catalyst for hydrogen evolution reaction. *Adv. Mater. Interfaces* **2017**, *4*, 1600825.
(40) Mu, C.; Qi, H.; Song, Y.; Liu, Z.; Ji, L.; Deng, J.; Liao, Y.; Scarpa, F. One-pot synthesis of nanosheet-assembled hierarchical $MoSe_2$/$CoSe_2$ microcages for the enhanced performance of electrocatalytic hydrogen evolution. *RSC Adv.* **2016**, *6* (1), 23−30.
(41) Ambrosi, A.; Sofer, Z.; Pumera, M. 2H → 1T phase transition and hydrogen evolution activity of MoS_2, $MoSe_2$, WS_2 and WSe_2 strongly depends on the MX_2 composition. *Chem. Commun.* **2015**, *51* (40), 8450−8453.

DOI: 10.1021/acssuschemeng.7b01181
ACS Sustainable Chem. Eng. 2017, 5, 6994−7002